(0001) Interfaces between M2O3 corundum oxides (M = Al, Ti, V, Cr, Fe).

H.-L.T. Le, J. Goniakowski, C. Noguera

Highlights

- Fundamental analysis of transition metal corundum oxide interfaces with DFT+U calculations
- Redox reaction at Ti_2O_3/V_2O_3 and Ti_2O_3/Fe_2O_3 interfaces driven by band off-sets
- Additional weaker electron transfer follows the difference of ionicity of parent oxides
- Interface stability can be deduced from energetics of corresponding mixed bulk oxides

(0001) interfaces between M_2O_3 corundum oxides (M = Al, Ti, V, Cr, Fe).

H.-L. T. Le[a], J. Goniakowski[a], C. Noguera[a]

[a] *CNRS-Sorbonne Université, UMR 7588, INSP, F-75005 Paris, France*

Abstract

The structural quality of oxide/oxide interfaces, their chemistry, and the nature of their electronic states are critical properties for new promising applications and require continuous advances in their fundamental understanding. To this goal, we have performed a theoretical study of a series of (0001) M_2O_3/M'_2O_3 interfaces (M, M' = Al, Ti, V, Cr, Fe) between simple and transition metal oxides crystallizing in the corundum structure. Our DFT+U results reveal two qualitatively different mechanisms of interface charge redistribution: an interfacial oxidation-reduction reaction occurring at Ti_2O_3/V_2O_3 and Ti_2O_3/Fe_2O_3 contacts, and a much weaker electron transfer along anion-cation bonds which follows the difference of ionicity between the two constituting oxides at all interfaces. At variance with interfaces between *sp* semiconductors, the band bending does not propagate beyond one or two atomic layers. More generally, our results show that the nature of the interface electronic structure and the energetics of its formation can be tightly linked to the properties of the corresponding bulk oxides, thus providing a precious tool for designing oxide/oxide interfaces of required characteristics.

Keywords: transition metal corundum oxides; oxide/oxide interfaces; DFT+U calculations; interfacial redox reaction; band off-sets; ionicity

1. Introduction

Oxides have long been used in a variety of applications, including catalysis, electronics and optoelectronics, or as thermal or electrical insulating barriers. More recently, all-oxide electronic devices have progressively replaced many of those traditionally based on semiconductors. In these fields, the structural quality of oxide/oxide interfaces, their precise composition, and the nature of their electronic states play a decisive role. It is also worth mentioning a more fundamental interest in oxide interfaces triggered by the discovery of emergent phenomena associating charge, spin and orbital degrees of freedom [1].

Despite this wide context, there are very few systematic studies of oxide/oxide interfaces which try to relate their characteristics to those of the constituting oxides. The most significant ones concern perovskite oxides [2] or the Cr_2O_3/Fe_2O_3 interface [3, 4, 5, 6]. Here our goal was to perform a thorough and systematic study of six (0001) interfaces between transition metal corundum oxides, including Ti_2O_3, V_2O_3, Cr_2O_3 and Fe_2O_3. We have also considered an hypothetical Ti_2O_3/Al_2O_3 interface as to include a more ionic oxide with pure *sp* character. Using a DFT+U approach, we have analyzed the nature of the states close to the Fermi level, the interface charge transfers, and the formation of interfacial dipoles. We link these interface characteristics to the band alignment between the constituting oxides and their difference in ionicity. Moreover, we evidence strong similarities between the energetics of M_2O_3/M'_2O_3 interfaces and the formation energies of mixed $MM'O_3$ oxides of corundum-type structures.

The paper is organized in the following way. After a section describing the computational methods and settings (Section 2), we summarize the results on anionic-type and cationic-type interfaces (Section 3). A discussion (Section 4) highlights two qualitatively different mechanisms of interface charge redistribution, both characterized by extremely short penetration lengths, and establishes a direct link between the interface stability and the

tendency for cationic mixing in the corresponding bulk corundum-type oxides. A conclusion follows (Section 5).

2. Computational details

DFT calculations are performed with the Vienna Ab-initio Simulation Package (VASP) [7, 8] using the Projector Augmented Wave (PAW) method [9, 10] to represent the electron-core interaction and a 400 eV energy cutoff in the development of Kohn-Sham orbitals on a plane-wave basis set. Transition metal $3p$ states are systematically considered as semi-core states. The DFT+U approach proposed by Dudarev [11, 12] is used together with the dispersion-corrected exchange-correlation functional (optB88-vdW) [13, 14, 15], as to improve the description of interfacial electronic structure and energetics. As in our previous work [16], we use U values equal to 1.0, 1.7, 3.0, and 3.0 for Ti_2O_3, V_2O_3, Cr_2O_3, and Fe_2O_3, respectively, which correctly account for the electronic characteristics of the bulk oxides. All calculations are spin-polarized and the non-magnetic (NM for Al_2O_3 and Ti_2O_3), G-type (for Cr_2O_3 and V_2O_3) and C-type (for Fe_2O_3) antiferromagnetic (AF) ground state orderings computed for the corresponding bulk materials [16] are systematically preserved. Ionic charges are estimated with the partition scheme proposed by Bader [17, 18] and magnetic moments are obtained by integration of the spin density within the Bader's volumes. Bulk and interface configurations are plotted with VESTA [19].

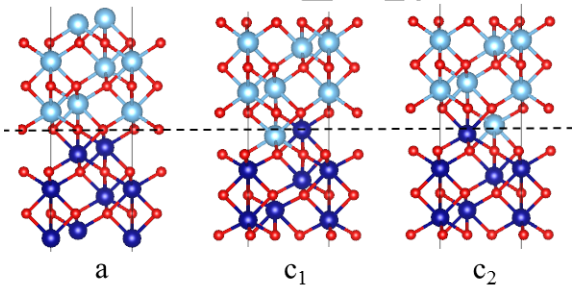

Figure 1: Atomic structure at anionic (a) and cationic (c_1 and c_2) interfaces. Oxygen and metal atoms are represented with red and blue (dark or light) balls, respectively.

Three types of interfaces are considered, involving either an interfacial oxygen layer (Figure 1, left, labeled a or *anionic* in the following), or an interfacial cationic bi-layer (Figure 1, right, labeled c_1 and c_2 or *cationic*). At a interfaces, the interfacial atoms are all equivalent, with two cation first neighbors of one type and two of the other. On each side of this layer, the two cations are nonequivalent. One is linked via a short inter-plane bond to a cation of its own type ("bulk-like" bond) and one with a cation of opposite type ("interfacial" bond). At c interfaces, a cation of a given type may occupy two inequivalent positions. In the configuration c_1, an interfacial cation has three in-plane first neighbors, zero inter-plane first neighbor and six inter-plane second neighbors with cations of opposite type. In the second configuration (noted c_2) in which the two interfacial cations have exchange positions, an interfacial cation has three in-plane first neighbors, one inter-plane first neighbor and three inter-plane second neighbors with cations of opposite type. In both cases, the oxygen atoms which are the closest to the interface have three cations first neighbor of one type and one of the other type, instead of having four cations first neighbors of the same type in the bulk. It should be noted that all anionic and cationic interfaces are non-polar [20]. Indeed, their repeat units of respective composition $O_{1.5}/M_2/O_{1.5}$ (for the anionic interface) and $M/O_3/M$ (for the cationic interfaces) bear no dipole moment and thus do not produce a polarization discontinuity [21].

Interfaces are represented by superlattices with six M_2O_3 formula units of each oxide, with an interface registry which preserves the corundum stacking. We have checked that alternative registries produce less stable configurations. The in-plane lattice parameters are fixed at the average values between those of the two corresponding bulks (4.80 Å, 5.14 Å, 5.05 Å, 5.04 Å, 5.06 Å, for bulk Al_2O_3, Ti_2O_3, V_2O_3, Cr_2O_3, and Fe_2O_3, respectively [16]), and the out-of-plane parameters are optimized until the corresponding components of stress tensor are smaller than 0.01 eV Å^{-3}. In addition, all atomic position are relaxed until maximum forces get smaller than 0.01 eV Å^{-1}. The Brillouin zone of the (1×1) interface unit cell is sampled on a Γ-centered $(8 \times 8 \times 1)$ Monkhorst-Pack grid [22].

The stability of an M_2O_3/M'_2O_3 interface is estimated from the interface energy E_{int}:

$$E_{int} = \frac{(E_{M_2O_3/M'_2O_3} - (E'_{M_2O_3} + E'_{M'_2O_3}))}{2S} \quad (1)$$

in which $E_{M_2O_3}$, $E_{M'_2O_3}$ are the energies of six formula units of bulk M_2O_3 and M'_2O_3 materials (at the average in-plane lattice parameter),

$E_{M_2O_3/M'_2O_3}$ is the energy of the constituted heterostructure, and S is the interface area. Factor 2 accounts for the two equivalent interfaces in the unit cell.

3. Results

In this section, the numerical results for the anionic and cationic interface structures are reported. We start by a comprehensive description of the cationic interfaces, and, in a second step, we highlight their similarities and differences with the anionic interfaces.

3.1. Cationic interfaces

Table 1 summarizes the electronic, magnetic and energetic properties of the most stable cationic configurations for all interfaces under consideration. Figures 2 and 3 display their local density of states (LDOS) projected on the cations at the interface and in bulk-like positions.

All interfaces are subject to similarly weak structural distortions since the lattice mismatch between the constituent oxides never exceeds 1.5%, except between Ti_2O_3 and Al_2O_3 for which it reaches 7%. At variance, the interface electronic structures display much bigger differences with respect to their bulk counterparts. On the one hand, at the Ti_2O_3/V_2O_3 and Ti_2O_3/Fe_2O_3 interfaces, a strong charge redistribution takes place between the two interfacial cations. It changes their oxidation states and thus can be seen as a local reduction-oxidation (redox) reaction. These two interfaces are also characterized by large negative interface energies. On the other hand, much smaller but not negligible interface charge rearrangements are also present at the five other interfaces. They principally reflect the charge modifications of the anions and systematically produce positive interface energies. A detailed presentation of the results for these two sets of interfaces is given in the following.

In the case of Ti_2O_3/V_2O_3 and Ti_2O_3/Fe_2O_3 interfaces which are characterized by a strong electron redistribution, the clearest and most consistent information can be deduced from the LDOS, Fig. 2, and magnetic moments, Tab. 1. Indeed, in the Ti_2O_3/Fe_2O_3 LDOS, the bulk-like Ti LDOS peak just below E_F has lost most of its weight on the interface Ti, implying a loss of formally one electron and thus a formal Ti^{+4} oxidation state. In parallel, the interfacial Fe-projected LDOS displays an additional filled peak compared to the bulk one, thus

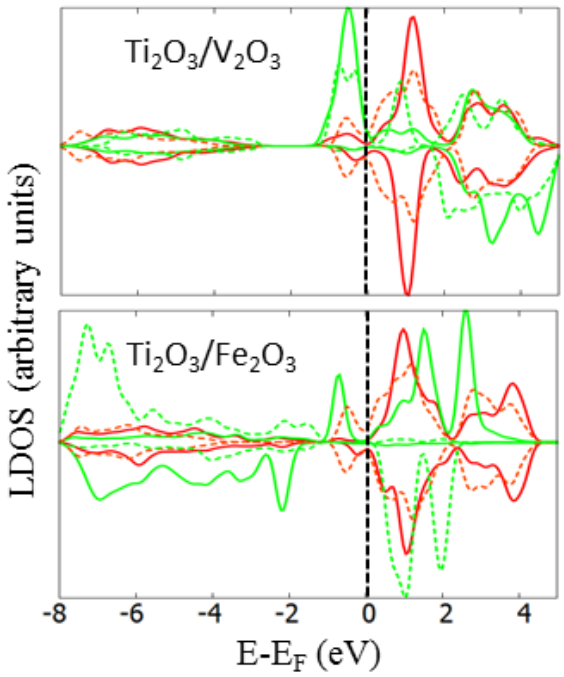

Figure 2: Densities of states projected on interfacial (plain lines) and bulk-like (dashed lines) cations at cationic M_2O_3/M'_2O_3 interfaces: Ti_2O_3/V_2O_3 and Ti_2O_3/Fe_2O_3. Red and green colors refer to M and M' cations, respectively.

Table 1: Characteristics of constituting bulk M_2O_3 and M'_2O_3 oxides (at average in-plane lattice parameter) and of the most stable cationic (c_1 or c_2) and anionic (a) M_2O_3/M'_2O_3 interfaces: Bader charges of cations Q_M and oxygen atoms Q_O (e), cation magnetic moments μ_M (μ_B). Total Bader charges Q_{int} of each side of the interface (e) and interface energies E_{int} (J/m^2).

	Ti_2O_3	Al_2O_3	Ti_2O_3/Al_2O_3 (c_1)	Ti_2O_3/Al_2O_3 (a)
Q_M	1.90	2.49	1.84, 1.98/2.50	1.97, 1.93/2.50
μ_M	0.0	0.0	0.0,0.0/0.0	0.0/0.0
Q_O	-1.27	-1.66	-1.39/-1.56	-1.48
Q_{int}	-	-	-0.33/+0.33	-0.29/+0.29
E_{int}	-	-	0.25	0.27
ine	Ti_2O_3	V_2O_3	Ti_2O_3/V_2O_3 (c_1)	Ti_2O_3/V_2O_3 (a)
Q_M	1.91	1.84	2.02, 2.10/1.62,1.72	2.01, 2.02 / 1.75, 1.86
μ_M	0.0	1.8	0.3, 0.0/2.3,2.1	0.3, 0.1 / 2.0, 2.0
Q_O	-1.27	-1.23	-1.26/-1.24	-1.28
Q_{int}	-	-	+0.44/-0.44	+0.27 / -0.27
E_{int}	-	-	-0.28	-0.18
ine	Ti_2O_3	Cr_2O_3	Ti_2O_3/Cr_2O_3 (c_1)	Ti_2O_3/Cr_2O_3 (a)
Q_M	1.91	1.77	2.01/1.69	1.96 / 1.73, 1.77
μ_M	0.0	2.9	0.4/3.0	0.7, 0.5 / 3.0, 2.8
Q_O	-1.27	-1.18	-1.25/-1.21	-1.24
Q_{int}	-	-	+0.20/-0.20	+0.14/-0.14
E_{int}	-	-	0.15	0.10
ine	Ti_2O_3	Fe_2O_3	Ti_2O_3/Fe_2O_3 (c_2)	Ti_2O_3/Fe_2O_3 (a)
Q_M	1.92	1.74	2.03,2.15 / 1.44, 1.49	2.08, 2.05 / 1.66, 1.50
μ_M	0.0	4.1	0.1 / 3.7	0.2, 0.1 / 3.9, 3.7
Q_O	-1.28	-1.16	-1.23/-1.18	-1.21
Q_{int}	-	-	+0.68/-0.68	+0.47/-0.47
E_{int}	-	-	-0.65	-0.45
ine	V_2O_3	Cr_2O_3	V_2O_3/Cr_2O_3 (c_1)	V_2O_3/Cr_2O_3 (a)
Q_M	1.84	1.77	1.86 / 1.76	1.86, 1.87 / 1.77, 1.77
μ_M	1.7	2.9	1.8 / 2.8	1.7, 1.8 / 2.9
Q_O	-1.22	-1.18	-1.22 /-1.20	-1.21
Q_{int}	-	-	+0.08/-0.08	+0.06/-0.06
E_{int}	-	-	0.02	0.01
ine	V_2O_3	Fe_2O_3	V_2O_3/Fe_2O_3 (c_2)	V_2O_3/Fe_2O_3 (a)
Q_M	1.85	1.74	1.96 /1.66	1.90, 1.84 / 1.76, 1.74
μ_M	1.7	4.1	1.5 / 4.0	1.6, 1.8 / 4.1, 4.1
Q_O	-1.23	-1.16	-1.22/-1.19	-1.21
Q_{int}	-	-	+0.15/-0.15	+0.08/-0.08
E_{int}	-	-	0.10	0.13
ine	Cr_2O_3	Fe_2O_3	Cr_2O_3/Fe_2O_3 (c_2)	Cr_2O_3/Fe_2O_3 (a)
Q_M	1.77	1.74	1.79 / 1.76	1.79, 1.77 / 1.78, 1.76
μ_M	2.9	4.1	2.9 /4.1	2.8, 2.9 / 4.1, 4.1
Q_O	-1.18	-1.16	-1.18 /-1.18	-1.19/-1.17
Q_{int}	-	-	+0.02/-0.02	-0.00/+0.00
E_{int}	-	-	0.12	0.16
ine				

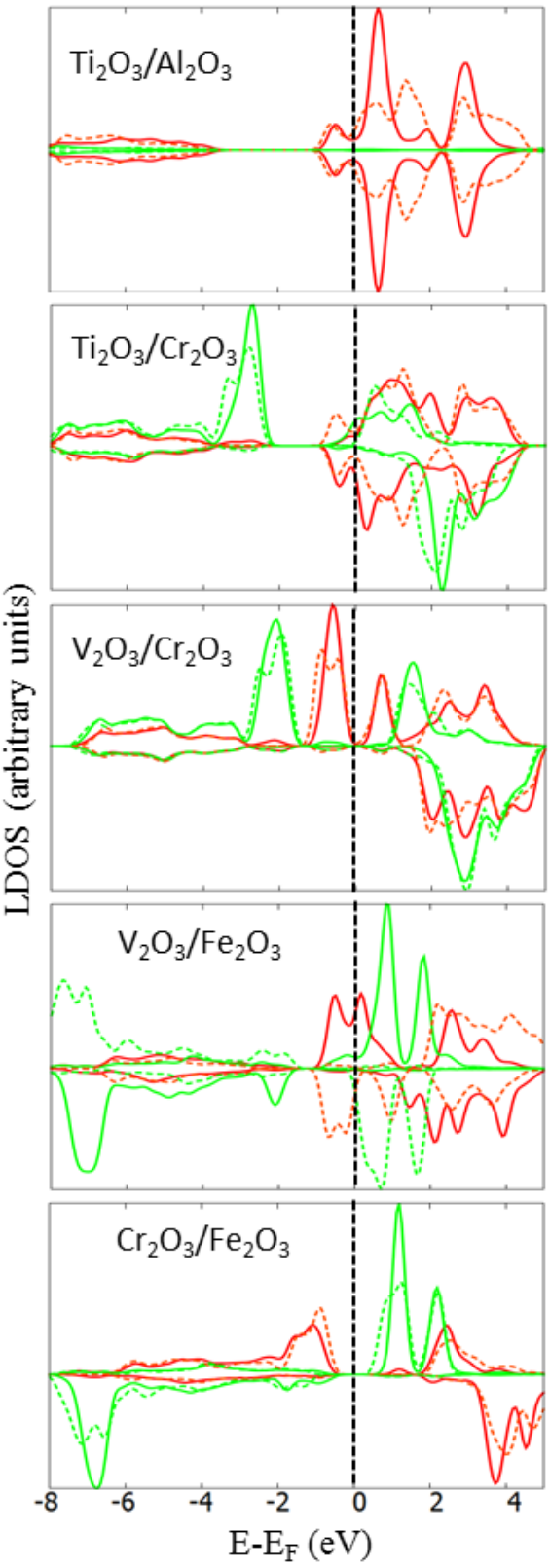

Figure 3: Same as Fig. 2 for cationic M_2O_3/M'_2O_3 interfaces: Ti_2O_3/Al_2O_3, Ti_2O_3/Cr_2O_3, V_2O_3/Cr_2O_3, V_2O_3/Fe_2O_3, and Cr_2O_3/Fe_2O_3.

pointing to a Fe^{2+} formal oxidation state. This analysis is further confirmed by the vanishing value of μ_{Ti}, characteristic of Ti^{+4} in the absence of the Ti-Ti bonding responsible for the NM ground state in bulk Ti_2O_3[16], and by the reduced magnetic moment on the interfacial Fe cation. Interestingly, a second cation on each side of the interface also experiences a change of oxidation state. The modifications of electronic structure lead to similar conclusions at the Ti_2O_3/V_2O_3 interface, with a strong increase of μ_V from 1.8 μ_B in the bulk to 2.3 μ_B on the interfacial vanadium atom and to 2.1 μ_B on one of the sub-interfacial vanadium atom. One should note that, at variance with *sp*-type semiconductor interfaces, an overlap between the narrow *d* states at the gap edges of these Mott-Hubbard oxides easily induces correlated shifts of whole *d* states across the Fermi level and, consequently, an actual oxydo-reduction process. In that case, it is thus legitimate to talk of a change of cation oxidation states.

Consistently with this change, the titanium charges increase at these two interfaces and those of vanadium and iron atoms are reduced ($\approx \pm 0.2$ at Ti_2O_3/V_2O_3 and $\pm 0.25 - 0.30$ at Ti_2O_3/Fe_2O_3). While the Bader charges do not give a direct information on formal charges, these variations are much larger than those at any of the remaining interfaces.

Finally, the changes of cation oxidation states deduced from the interface electronic structure are consistent with local structural modifications. Indeed, the interfacial Ti-O bond-lengths are shortened and the V-O and Fe-O expanded by $\approx \pm 0.1$ Å, respectively, in line with the dependence of ionic radii on ionic charges ($r_{M^{4+}} < r_{M^{3+}} < r_{M^{2+}}$) [23].

In the second set of interfaces, characterized by weaker electron redistributions, the cation oxidation states can also be deduced from the LDOS, Fig.3, and magnetic moments, Tab. 1. In particular, at the Ti_2O_3/Al_2O_3, V_2O_3/Cr_2O_3 and Cr_2O_3/Fe_2O_3 interfaces, the interfacial and bulk cations have quasi-identical LDOS in the Fermi level vicinity and their magnetic moments are very close to each other, clearly showing that the cation bulk 3+ oxidation state is maintained at both sides of the interface.

At the Ti_2O_3/Cr_2O_3 and V_2O_3/Fe_2O_3 interfaces, the metallic character of the electronic structure originating from hybridized cation states at E_F does not allow to unambiguously assign oxidation states to the interfacial cations. For example, at the Ti_2O_3/Cr_2O_3 interface, the filled Ti peak below the Fermi level is up-shifted and partially de-

pleted while, concomitantly, the Cr peak localized above E_F in bulk Cr_2O_3 moves to lower energies, suggesting a small but non-vanishing electron redistribution between Ti and Cr, associated to small variations of the cation magnetic moments (≈ 0.15 μ_B) and Bader charges (≈ 0.1 e).

Interestingly, while the cation charges are hardly modified at these five interfaces except when a small cation-cation hybridization takes place, the charges of interfacial oxygen atoms display larger variations. At each M_2O_3/M'_2O_3 interface, they are close to an average of the bulk charges, $Q_O \approx (3Q_O(M_2O_3) + Q_O(M'_2O_3))/4$ on the M_2O_3 side and $Q_O \approx (Q_O(M_2O_3) + 3Q_O(M'_2O_3))/4$ on the M'_2O_3 side, consistently with their numbers of O-M and O-M' bonds.

To summarize, we find that structural distortions at cationic interfaces are systematically small, except in the case of Ti_2O_3/Al_2O_3, where the lattice mismatch between the two oxides is larger or when a redox reaction takes place. The latter occurs only at the Ti_2O_3/V_2O_3 and Ti_2O_3/Fe_2O_3 interfaces. The local redox reaction $Ti^{3+} + M^{3+} \longrightarrow Ti^{4+} + M^{2+}$ (M = V, Fe) results in strong modifications of the interfacial cation characteristics, and is associated with negative interface energies. At variance, at all other interfaces, the electronic rearrangements are much weaker. They mainly affect the charges on the interfacial oxygen atoms, and are associated with positive interface energies.

3.2. Anionic interfaces

Despite their different atomic structure, Fig. 1, anionic interfaces share many common characteristics with the cationic ones, Tab. 1. In particular, this concerns the presence of the interfacial redox reaction and the negative interface energy at the very same two interfaces (Ti_2O_3/V_2O_3 and Ti_2O_3/Fe_2O_3), and the much weaker electronic rearrangements associated with positive interface energies in all the remaining cases. In the following we describe the features which are specific to these two sets of anionic interfaces.

At the Ti_2O_3/V_2O_3 and Ti_2O_3/Fe_2O_3 interfaces, the redox reaction only induces a partial cation-to-cation electron exchange. At the Ti_2O_3/Fe_2O_3 interface, the LDOS of the two interfacial Ti atoms are nearly identical, Fig. 4, each with approximately a half-emptied peak at the Fermi level. Similarly, the additional Fe state below E_F involves the two interfacial Fe ions, although unequally. This suggests that a single electron is exchanged across the anionic interface, and that the transferred charge is shared between the two Ti and the two Fe on each side of the interface. Conversely, at the Ti_2O_3/V_2O_3 interface, the filling of the Ti state just below E_F is slightly larger than at the Ti_2O_3/Fe_2O_3 junction, and the Fermi level intercepts a vanadium state localized on a single interfacial vanadium atom. At both interfaces, the Ti-O bond-lengths are shortened and the V-O or Fe-O bondlengths are expanded by ≈ 0.1 Å. However, the variations of the cation magnetic moments with respect to the bulks are less pronounced than at the cationic interfaces. Due to the metallic character of the Ti_2O_3/V_2O_3 electronic structure and the sharing of the transferred electron between two Ti and two Fe atoms at the Ti_2O_3/Fe_2O_3 interface, it is not possible to assign formal oxidation states to the interfacial cations as unambiguously as at the corresponding cationic interfaces.

Electronic and magnetic characteristics of the other five anionic interfaces (Ti_2O_3/Al_2O_3, Ti_2O_3/Cr_2O_3 V_2O_3/Cr_2O_3, V_2O_3/Fe_2O_3, and Cr_2O_3/Fe_2O_3) are extremely close to those at the corresponding cationic interfaces. Only the interfacial oxygen charges are visibly different, due to their different local environment. They are close to the average of bulk values $Q_O \approx (Q_O(M_2O_3) + Q_O(M'_2O_3))/2$ with a 1:1 ratio corresponding to their equal number of O-M and O-M' bonds with the neighboring cations.

To summarize, anionic interfaces present many electronic and energetic similarities with cationic interfaces. However, the strong electron transfer occurring at the Ti_2O_3/V_2O_3 and Ti_2O_3/Fe_2O_3 interfaces remains limited to one electron per unit cell or less, shared between two cations of each type. At variance with cationic interfaces, it cannot be unambiguously transcribed into well-defined changes of cation oxidation states.

4. Discussion

In this section, we highlight two qualitatively different mechanisms of interface charge redistribution, both characterized by extremely short penetration lengths, and we establish a direct link between the interface stability and the tendency for cationic mixing in the corresponding bulk corundum-type oxides.

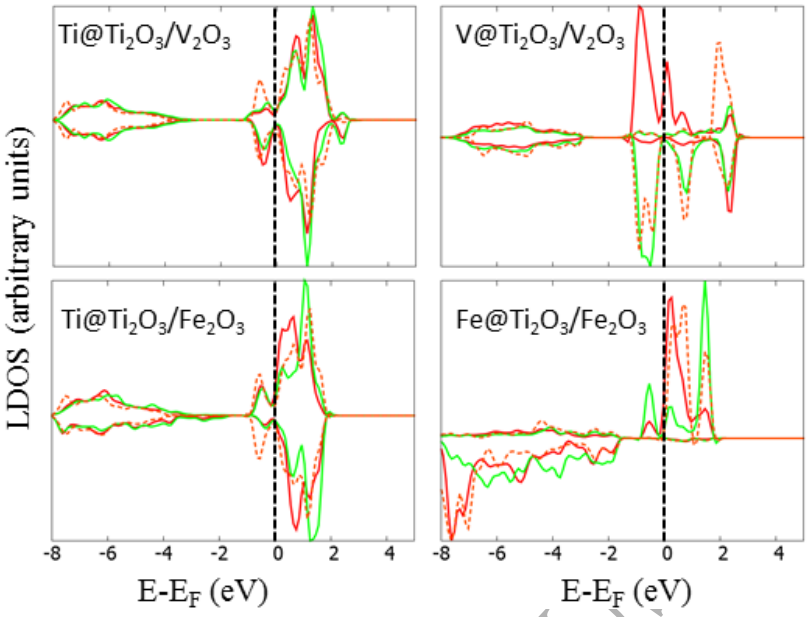

Figure 4: Densities of states projected on interfacial (plain lines) and bulk-like (dashed lines) cations at Ti_2O_3/V_2O_3 and Ti_2O_3/Fe_2O_3 oxygen interfaces. Red and green colors refer to the two inequivalent interface cations of each type.

4.1. Cation-to-cation interfacial charge transfer

An understanding of charge transfers and dipole formation at interfaces is usually obtained by aligning the band structures of the two materials with respect to a common reference energy [2, 24, 25, 26, 27, 28, 29, 30, 31]. In the present case of M_2O_3/M'_2O_3 interfaces, the most natural choice is the energy of the oxygen 1*s* states of the two oxides.

Actually, we have recently used a similar strategy to tackle the question of cation-to-cation electron transfer in a different context. We have considered mixed $MM'O_3$ compounds involving the same cations (M, M' = Al, Ti, V, Cr, and Fe) in bulk corundum-like structures, such as the ilmenite and the $LiNbO_3$ ones [16]. By comparing the electronic characteristics of the mixed $MM'O_3$ oxides with those of their M_2O_3 and M'_2O_3 pure parents, we have unambiguously identified the presence of a mixing-induced redox reaction in the case of $TiVO_3$ and $TiFeO_3$, leading to Ti^{4+}, V^{2+} and Fe^{2+} oxidation states. Conversely, in all other mixed $MM'O_3$ compounds, the cations remained in the 3+ oxidation state characteristic of the pure oxides. In the same study, relying on an alignment of the oxygen 1*s* levels of the parent oxides, we have pointed out that the existence of the redox reaction in $TiVO_3$ and $TiFeO_3$ only, results from the particularly elevated position of the valence band maximum of Ti_2O_3 associated with its strong Mott-Hubbard character, which overlaps the conduction band minima of V_2O_3 and Fe_2O_3 [16].

These results are perfectly consistent with the present ones and show that, despite the misfit-induced distortions, the specificity of the Ti_2O_3 electronic structure remains the principal factor which determines the occurrence of a redox reaction at the Ti_2O_3/M'_2O_3 interfaces (M'=V, Fe), for which the offset between the parent materials is the largest [16]. At these cationic interfaces, two electrons are transferred per unit cell, leading to a change of oxidation state of two cations on each side of the interface. The electron transfer, limited to a single electron per unit cell, is smaller at the corresponding anionic interfaces.

4.2. Anion-to-cation interfacial charge transfer

Aside from the strong cation-to-cation electron exchange found at the Ti_2O_3/V_2O_3 and Ti_2O_3/Fe_2O_3 junctions, a second mechanism of charge redistribution exists at oxide/oxide interfaces. Indeed, as summarized in Tab.1, a smaller, but non-vanishing interfacial charge transfer $\pm Q_{int}$, is also systematically present, even in the absence of redox reaction. It is mainly due to the charge modifications of the oxygen atoms bound to both M and M' cations with respect to their values in

pure M_2O_3 and M'_2O_3 oxides, as noted in Section 3. For example, at the cationic Ti_2O_3/Al_2O_3 junction, the interfacial oxygen atoms on the Ti_2O_3 side bear more negative charges than in bulk Ti_2O_3 due to their bonding to Al ions, Tab. 1. This is the main reason for a significant electron transfer from Al_2O_3 towards Ti_2O_3 ($Q_{int} < 0$). Such a mechanism of charge redistribution exists at all interfaces but is partially hidden by the stronger cation-to-cation charge transfer when a redox reaction takes place.

Interestingly, the variations of Q_{int} along the series of M_2O_3/M'_2O_3 interfaces display similar trends, independently of the cationic or anionic character of the junctions. This concerns both the amplitude and the sign of Q_{int}, and suggests that it results from the difference between intrinsic characteristics of the two materials. Indeed, as highlighted in Tab. 2, we find that the values of Q_{int} correlate well with the difference δQ_O between the oxygen charge values in the two constituent bulk materials. It is thus the ionicity difference between the two oxides which drives the interfacial charge transfer Q_{int}. For example, the larger ionicity of Al_2O_3 compared to Ti_2O_3, is responsible for negative Q_{int} at the Ti_2O_3/Al_2O_3 interface. Conversely, at other M_2O_3/M'_2O_3 interfaces, since M_2O_3 is always somewhat more ionic than M'_2O_3 [16], Q_{int} is positive and much smaller. Small deviations from this general trend occur at the cationic V_2O_3/Fe_2O_3 interface due to a non-negligible V-Fe hybridization resulting in a small cationic contribution to Q_{int}.

4.3. Band bending at the interface

The band offsets at the interface or the difference in ionicity of the two oxides only drive the first step towards the formation of the interfacial dipole. Subsequent electron rearrangements take place in response to the electron transfers, so that the character and the penetration length of the overall dipolar layer are the result of a self-consistent procedure involving the band bending of electrostatic origin in the two materials.

In order to estimate the characteristic length at which the electronic structure of the two materials is affected by the presence of the interface, in Fig. 5 we have represented the variations of the total electrostatic potential at the oxygen cores across the anionic interfaces. In all cases, we find that the electron redistribution and the band bending are very strongly localized in the closest vicinity

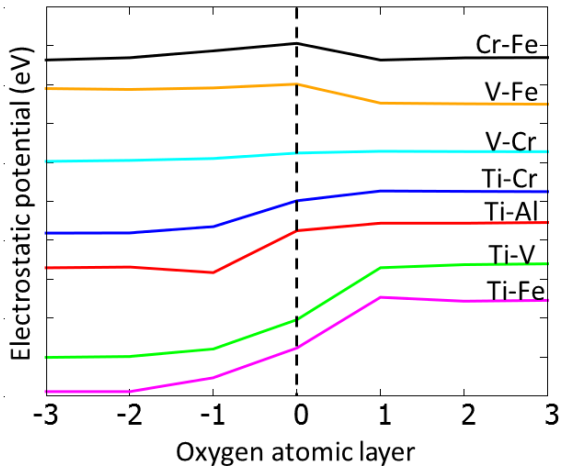

Figure 5: Variations of the electrostatic potential on oxygen atoms (three atoms on each side of the oxygen interfacial layer) across anionic M_2O_3/M'_2O_3 interfaces: Ti/Al (red), Ti/V (green), Ti/Cr (blue), Ti/Fe (pink), V/Cr (cyan), V/Fe (orange) Cr/Fe (black). The curves have been vertically shifted for the sake of clarity and the unit on the vertical energy scale is 1 eV. Lines are drawn to guide the eyes.

of the interface, so that the penetration length of the dipolar layer never exceeds one or two atomic layers. This is at variance with interfaces between *sp* semiconductors, and can be related to the ionic character of the oxides under consideration and the localized nature of their *d* orbitals compared to the *sp* ones.

4.4. Interface energies and mixing properties

In Tab. 3 we summarize the values of the interface energies E^c_{int} and E^a_{int} at the M_2O_3/M'_2O_3 cationic and anionic interfaces. We also recall the values of the bulk formation energies of mixed $MM'O_3$ oxides involving the same pairs of cations and estimated within the same DFT+U approach [16].

The reason to compare the energetics of mixed oxides and oxide/oxide interfaces lies in the similarity of their atomic structure and composition. Bulk ilmenite-type and $LiNbO_3$-type structures, which are represented in Fig. 6, are sub-groups of the bulk corundum structure, with M and M' cations ordered either into alternating pure {M,M} and {M',M'} bilayers (Fig. 6, left panel) or with mixed {M,M'} bilayers (Fig. 6, right panel) along the hexagonal c-axis. The layer structure in the vicinity of the anionic and cationic interfaces is reminiscent of a part of ilmenite and $LiNbO_3$ bulks, respectively.

Table 2: Charge transfers across cationic (c) and anionic (a) M_2O_3/M'_2O_3 interfaces (e/unit cell). Positive Q_{int} correspond to electron transfer from M_2O_3 to M'_2O_3. The Bader charges of the corresponding bulk oxygen atoms Q_O and Q'_O (e) [16] and their difference $\delta Q_O = Q_O - Q'_O$ (e) are recalled.

M_2O_3/M'_2O_3	Q^c_{int}	Q^a_{int}	δQ_O	Q_O	Q'_O
Ti_2O_3/Cr_2O_3	+0.20	+0.14	+0.09	-1.27	-1.18
V_2O_3/Fe_2O_3	+0.15	+0.08	+0.07	-1.23	-1.16
V_2O_3/Cr_2O_3	+0.08	+0.06	+0.05	-1.23	-1.18
Cr_2O_3/Fe_2O_3	+0.02	0.00	+0.02	-1.18	-1.16
Ti_2O_3/Al_2O_3	-0.33	-0.29	-0.39	-1.27	-1.66

Table 3: Calculated interface energies of cationic $E^{c_1}_{int}$, $E^{c_2}_{int}$ and anionic E^a_{int} M_2O_3/M'_2O_3 interfaces (eV/cell), formation energies of mixed $MM'O_3$ compounds in ilmenite-type E^{ilm}_{form} and $LiNbO_3$-type E^{LNO}_{form} structures (eV/formula unit), and the corresponding effective cation-cation mixing parameters W_1, W_2 and W_3 (see text) (eV), from Ref. [16].

	$TiFeO_3$	$TiVO_3$	$VFeO_3$	$VCrO_3$	$TiCrO_3$	$CrFeO_3$	$TiAlO_3$
ine $E^{c_1}_{int}$	-0.88	-0.40	0.36	0.02	0.21	0.28	0.33
$E^{c_2}_{int}$	-0.91	-0.31	0.13	0.06	0.35	0.17	0.70
E^a_{int}	-0.63	-0.25	0.18	0.01	0.14	0.22	0.36
ine E^{ilm}_{form}	-0.79	-0.35	-0.10	0.00	0.04	0.08	0.29
E^{LNO}_{form}	-0.73	-0.33	-0.01	0.02	0.16	0.06	0.60
ine W_1	-0.083	-0.043	0.017	0.010	0.052	0.022	0.118
W_2	-0.325	-0.125	-0.040	-0.015	-0.013	-0.048	0.223
W_3	-0.052	-0.025	-0.007	0.002	0.006	0.014	0.008

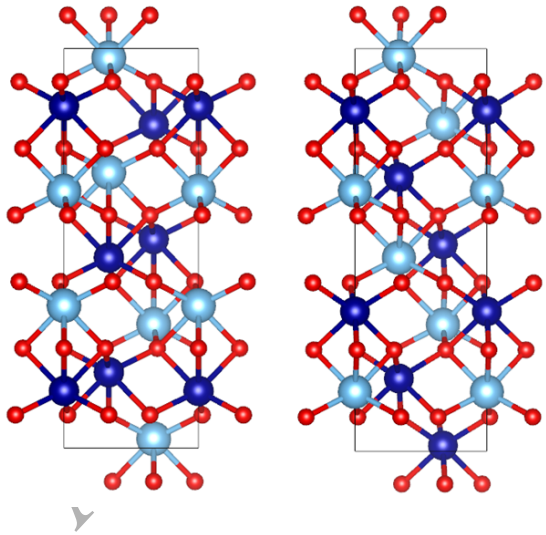

Figure 6: Unit cells for bulk $MM'O_3$ in the ilmenite (left) and $LiNbO_3$ (right) structures. Cations are represented as blue (light and dark) balls and oxygen atoms as red ones.

According to Tab. 3, the trends of interface and formation energies along the series of compounds show striking similarities. On the one hand, strongly negative energies are found for Ti_2O_3-Fe_2O_3 and Ti_2O_3-V_2O_3 systems, where redox reactions occur. Since negative interface energies indicate a preference to maximize the interface area, the mixed oxides in the ilmenite or $LiNbO_3$ structures can be seen as the ultimate limits of compounds uniquely composed of interfaces. These negative values are consistent with the fact that the ordered Ti_2O_3-Fe_2O_3 alloy at 50% composition is a well-known mineral (ilmenite) of chemical formula $TiFeO_3$ [32]. Moreover, although $TiVO_3$ does not naturally exist, it has been recently synthesized as a thin film on c-cut sapphire [33]. On the other hand, the largest positive energies are characteristic of Ti_2O_3-Al_2O_3, for which both the lattice mismatch and the difference of ionic character are the largest. In this case, much energy is required to form the interface and no mixing between the two oxides is expected, consistently with the absence of experimental evidence for $TiAlO_3$ alloys. Finally, smaller and mostly positive energies are systematically found in all other cases, where the electronic rearrangements upon interface or mixed compound formation are less noticeable.

In Ref. [16], we have analyzed the formation energies of the MM'O_3 compounds by introducing effective cation-cation mixing parameters $W_i = 2V_i^{MM'} - V_i^{MM} - V_i^{M'M'}$ associated to interaction energies V_i between same (MM or $M'M'$) and different (MM') cations in first ($i = 1$), second ($i = 2$), and third ($i = 3$) neighbor positions, Tab. 3 [16]. The structural similarity between mixed bulk and interface lattices makes it possible to express the interface energies in terms of the same mixing parameters:

$$\begin{aligned} E_{int}^{a} &= W_2 + 9W_3 \\ E_{int}^{c_1} &= 3W_1 + 12W_3 \\ E_{int}^{c_2} &= 3W_1 + 2W_2 + 12W_3 \end{aligned} \quad (2)$$

Figure 7 shows a comparison between the values of E_{int}^{a}, $E_{int}^{c_1}$ and $E_{int}^{c_2}$ obtained from the full DFT calculations and those approximated by Eq. 2, using the W_i values deduced from the MM'O_3 bulk simulations, Tab. 3. It turns out that, despite differences in the local environments of the atoms at the interface and in the mixed bulks, the overall trend is well reproduced, showing a good transferability of the effective cation-cation interactions. Due to the large number of first- ($i = 1$) and third-neighbor ($i = 3$) cation-cation pairs in the corundum structure, the formation energies of mixed bulks are principally driven by the W_1 and W_3 parameters. Equations 2 show that the same is true for the cationic and anionic interfaces, which explains the similar behaviors of E_{form} and E_{int} in the series, Tab. 3.

5. Conclusion

Relying on a DFT+U approach, we have studied a series of non-polar (0001) M_2O_3/M'$_2O_3$ interfaces between corundum bulk oxides of M_2O_3 stoichiometry (M = Al, Ti, V, Cr, Fe), with either an anionic or a mixed cation interfacial composition. We find that, regardless of the precise interface structure, two qualitatively different mechanisms of charge redistribution operate.

At Ti_2O_3/V_2O_3 and Ti_2O_3/Fe_2O_3 interfaces a reduction-oxidation reaction takes place, associated with a substantial cation-to-cation charge transfer, and resulting in a change of oxidation states of the interfacial cations. The effect is traced back to the overlap of the valence band maximum of Ti_2O_3 with the conduction band minima of V_2O_3 and Fe_2O_3. It produces large negative interface energies, consistent with the known stability of mixed $TiVO_3$ and $TiFeO_3$ oxides.

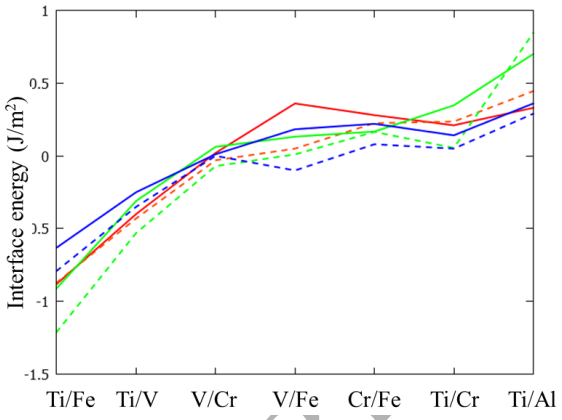

Figure 7: Calculated cationic c_1 (red), cationic c_2 (green) and anionic (blue) interface energies for the considered series of interfaces. Full and dashed lines represent the result of full DFT+U calculations and the estimation obtained with effective cation-cation mixing parameters W_i, Tab. 3, respectively.

While charge rearrangements are much less important at all the remaining interfaces, a non vanishing interface charge transfer is still found. It is mainly due to electron redistribution along anion-cation bonds and its sign and amplitude scale with the difference of ionicity between the two constituting oxides. These interfaces are mostly characterized by small positive interface energies.

Contrary to interfaces between *sp* semiconductors and regardless of the precise nature of the charge transfer, the penetration length of the interfacial band bending is limited to one or two atomic layers.

Strong similarities between the M_2O_3/M'$_2O_3$ interface energies and the energetics of formation of mixed MM'O_3 compounds in corundum-type structures have been demonstrated, and have been attributed to the transferable effective cation-cation interactions in these two types of systems. In particular, the substantially negative values of E_{int} at Ti_2O_3/V_2O_3 and Ti_2O_3/Fe_2O_3 interfaces are fully consistent with the known stability of ordered mixed $TiVO_3$ and $TiFeO_3$ compounds.

More generally, our results show that the nature of the interface electronic structure and the energetics of its formation can be tightly linked to the properties of the corresponding bulk oxides, thus providing a precious tool for designing oxide/oxide interfaces of required characteristics.

6. References

References

[1] H. Y. Hwang, Y. Iwasawa, M. Kawazaki, B. Keimer, N. Nagaosa, Y. Tokura, Emergent phenomena at oxide interfaces, Nature Materials 11 (2012) 103.

[2] Z. Zhong, P. Hansmann, Band alignment and charge transfer in complex oxide interfaces, Phys. Rev. X 7 (2017) 011023.

[3] S. A. Chambers, Y. Liang, Y. Gao, Noncummutative band offset at $\alpha-cr_2o_3/\alpha-fe_2o_3(0001)$ heterojunctions, Phys. Rev. B 61 (2000) 13223–13229.

[4] S. Chambers, J. Williams, M. Henderson, A. Joly, M. Varela, S. Pennycook, Structure, band offsets and photochemistry at epitaxial ?-cr2o3/?-fe2o3 heterojunctions, Surface Science 587 (2005) L197 – L207.

[5] J. E. Jaffe, M. Dupuis, M. Gutowski, First-principles study of noncommutative band offsets at $\alpha-cr_2o_3/\alpha-fe_2o_3(0001)$ interfaces, Phys. Rev. B 69 (2004) 205106.

[6] Y. Kota, H. Imamura, M. Sasaki, Enhancement of spin correlation in cr2o3 film above nel temperature induced by forming a junction with fe2o3 layer: First-principles and monte-carlo study, IEEE TRANSACTIONS ON MAGNETICS 50 (2014) 2540504.

[7] G. Kresse, J. Furthmuller, Efficient iterative schemes for ab initio total energy calculations using a plane-wave basis set, Phys. Rev. B 54 (1996) 11169–11186.

[8] G. Kresse, J. Hafner, Ab initio molecular dynamics for liquid metals, Phys. Rev. B 47 (1993) 558–561.

[9] P. E. Blöchl, Projector augmented-wave method, Phys. Rev. B 50 (1994) 17953–17979.

[10] G. Kresse, J. Joubert, From ultrasoft pseudopotentials to the projector augmented-wave method, Phys. Rev. B 59 (1999) 1758–1775.

[11] V. I. Anisimov, F. Aryasetiawan, A. I. Liechtenstein, First-principles calculations of the electronic structure and spectra of strongly correlated systems: the lda+u method, J. Phys.: Condens. Matter 9 (1997) 767–808.

[12] S. L. Dudarev, G. A. Botton, S. Y. Savrasov, C. J. Humphreys, A. P. Sutton, Electron-energy-loss spectra and the structural stability of nickel oxide:??an lsda+u study, Phys. Rev. B 57 (1998) 1505–1509.

[13] M. Dion, H. Rydberg, E. Schroder, D. C. Langreth, B. I. Lundqvist, Van der Waals density functional for general geometries, Phys. Rev. Lett. 92 (2004) 246401.

[14] J. Klimes, D. R. Bowler, A. Michaelides, Chemical accuracy for the van der Waals density functional, J. Phys.: Cond. Matt. 22 (2010) 022201.

[15] J. Klimes, D. R. Bowler, A. Michaelides, Van der Waals density functionals applied to solids, Phys. Rev. B 83 (2011) 195131.

[16] H.-L. T. Le, J. Goniakowski, C. Noguera, Properties of mixed transition metal oxides: $Mm'o_3$ in corundum-type structures (m, m' = al, ti, v, cr, and fe), Phys. Rev. Mat. 2 (2018) 085001.

[17] R. F. W. Bader, A quantum theory of molecular structure and its applications, Chem. Rev. 91 (1991) 983.

[18] G. Henkelman, A. Arnaldsson, H. Jonsson, A fast and robust algorithm for Bader decomposition of charge density, Comput. Mater. Sci. 36 (2006) 354–360.

[19] K. Momma, F. Izumi, Vesta 3 for three-dimensional visualization of crystal, volumetric and morphology data, J. Appl. Crystallogr. 41 (2011) 1272–1276.

[20] J. Goniakowski, F. Finocchi, C. Noguera, Polarity of oxide surfaces and nanostructures, Rep. Prog. Phys. 71 (2008) 016501.

[21] J. Goniakowski, C. Noguera, Conditions for electronic reconstruction at stoichiometric polar/polar interfaces, Journal of Physics: Condensed Matter 26 (2014) 485010.

[22] H. Monkhorst, J. Pack, Special points for brillouin-zone integrations, Phys. Rev. B 13 (1976) 5188–5192.

[23] R. D. Shannon, Revised effective ionic radii and systematic studies of interatomic distances in halides and chalcogenides, Acta Crystallogr. A 32 (1976) 751–767.

[24] R. L. Anderson, Experiments on ge-gaas heterojunctions, Solid-State Electron. 5 (1962) 341–351.

[25] W. R. Frensley, H. Kroemer, Theory of the energy-band lineup at an abrupt semiconductor heterojunction, Phys. Rev. B 16 (1977) 2642–2652.

[26] C. G. V. de Walle, R. M. Martin, Theoretical study of band offsets at semiconductor interfaces, Phys. Rev. B 35 (1987) 8154–8165.

[27] W. A. Harrison, Electronic Structure and the Properties of Solids, Freeman, San Francisco, 1980.

[28] S. Massida, B. I. Min, A. J. Freeman, Interface phenomena at semiconductor heterojunctions: Local-density valence-band offset in gaas/alas, Phys. Rev. B 35 (1987) 9871–9874.

[29] C. Tejedor, F. Flores, A simple approach to heterojunctions, J. Phys. C 11 (1978) L19.

[30] F. Flores, C. Tejedor, Energy barriers and interface states at heterojunctions, J. Phys. C 12 (1979) 731.

[31] J. Tersoff, Theory of semiconductor heterojunctions: The role of quantum dipoles, Phys. Rev. B 30 (1984) 4874–4877.

[32] T. F. W. Barth, E. Posnjak, The crystal structure of ilmenite, Zeitschrift Kristallographie 88 (1934) 265–270.

[33] A. Kramer, E. Sutter, D. Su, M. Batzill, Epitaxial corundum-$vtio_3$ thin films grown on c-cut sapphire, Thin Solid Films 631 (2017) 85–92.